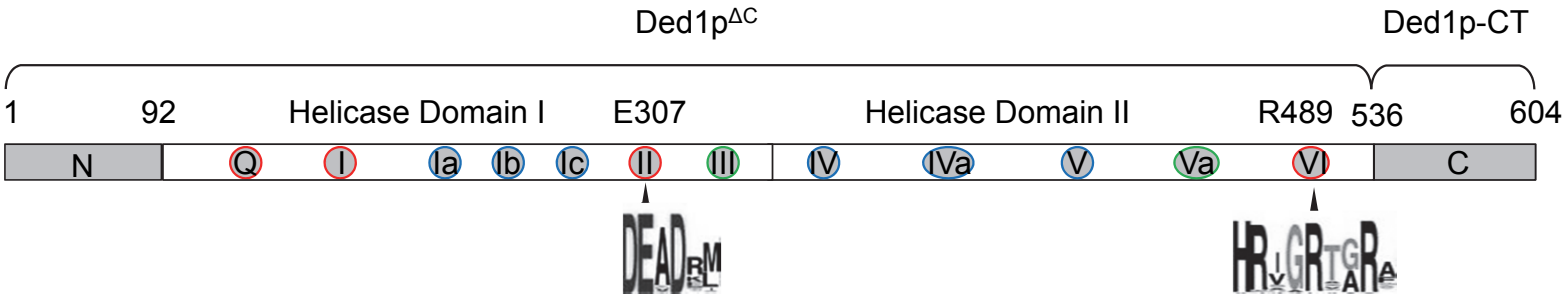

Supplementary Figure S1

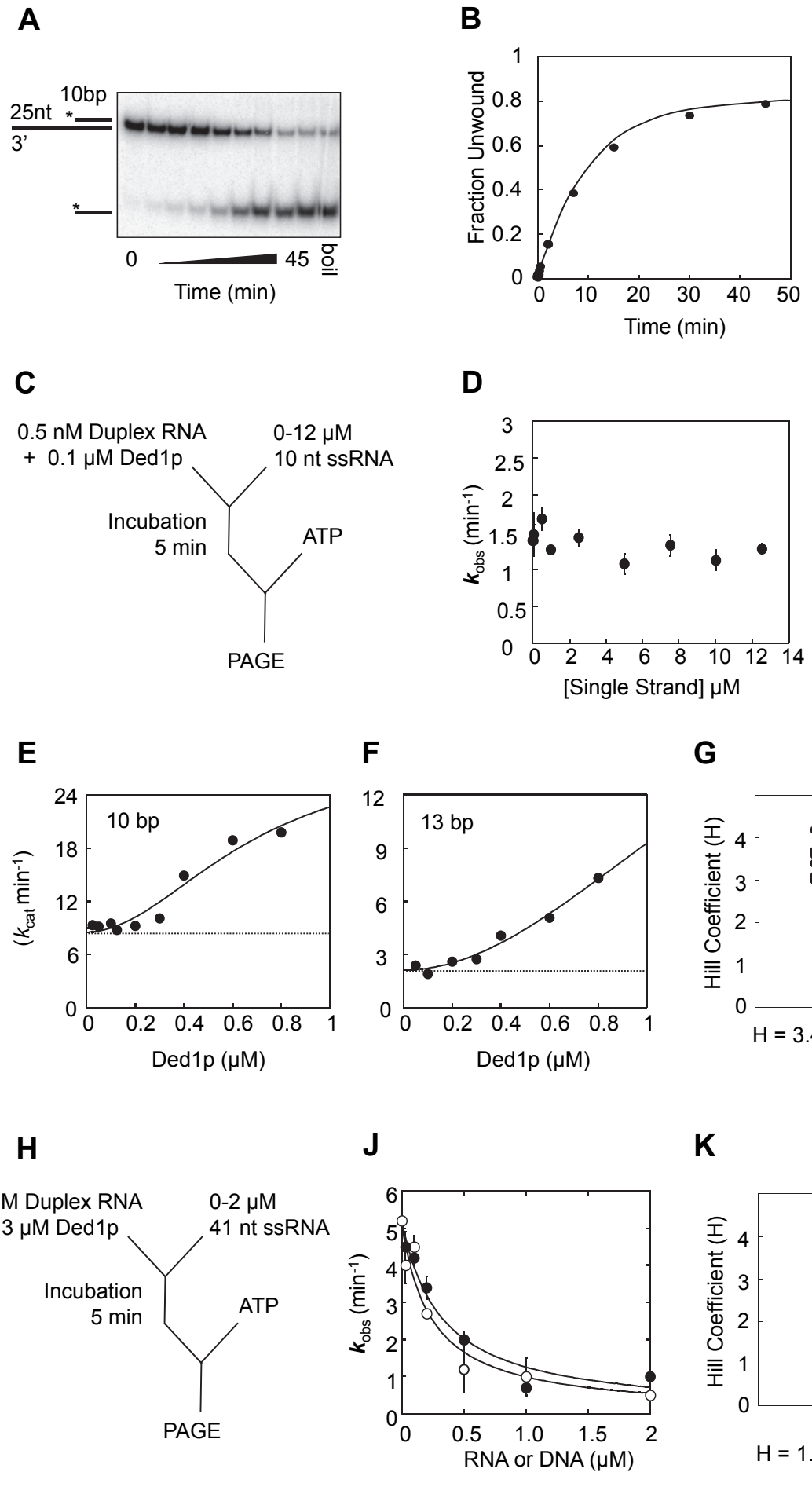

Supplementary Figure S2

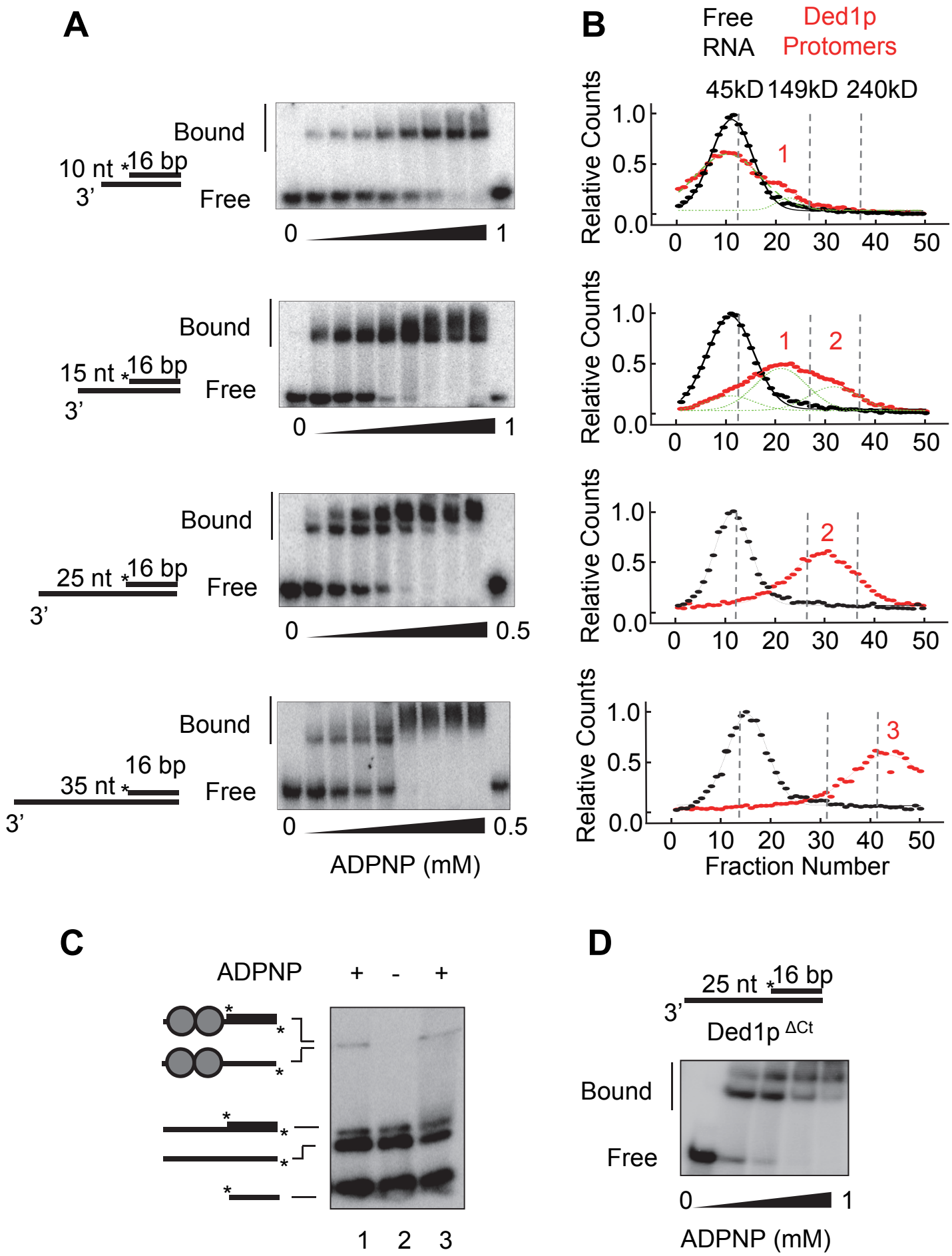

Supplementary Figure S3

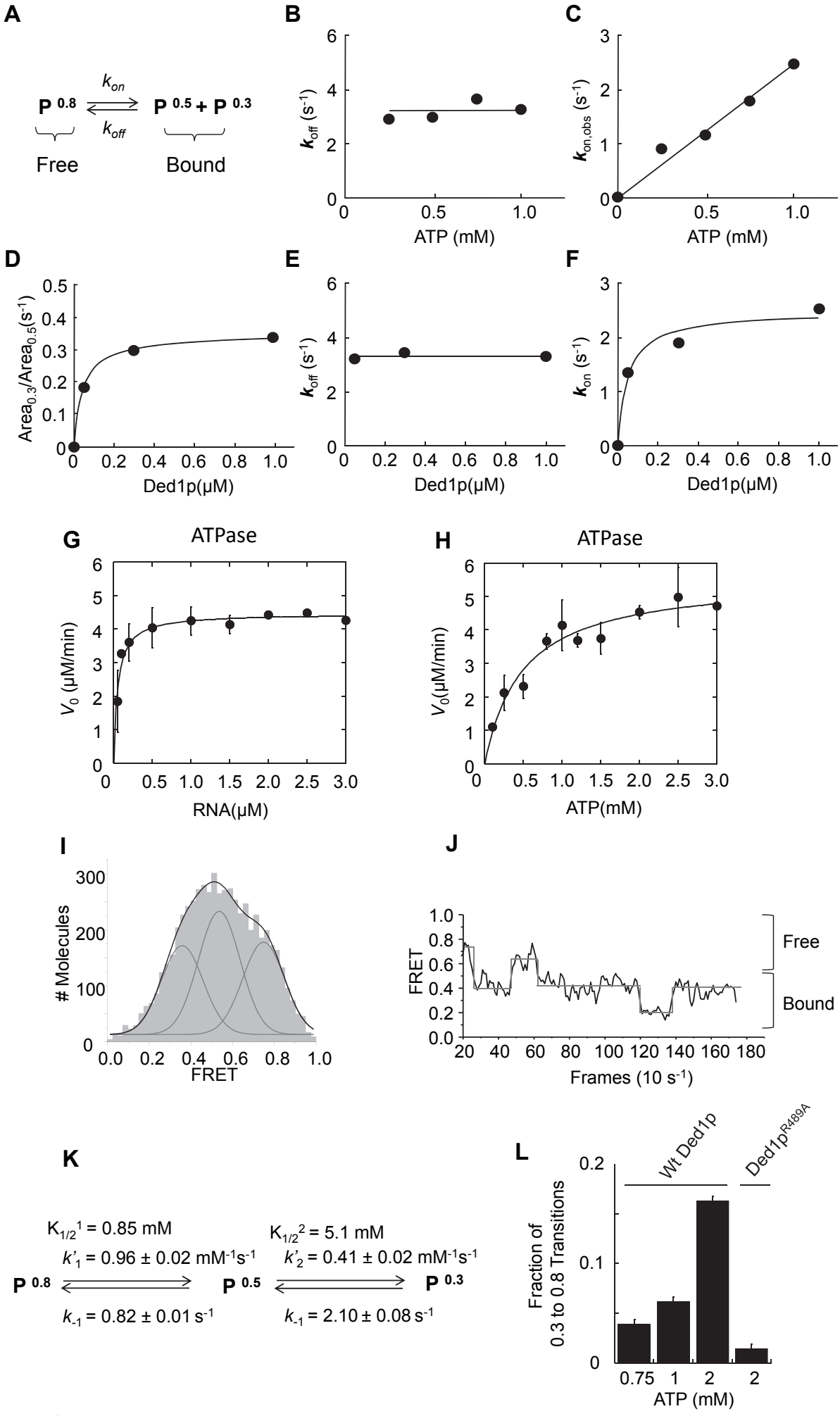

Supplementary Figure S4

A

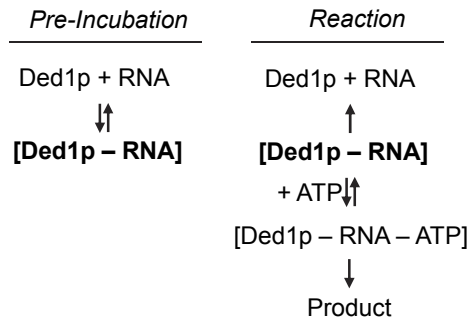

B

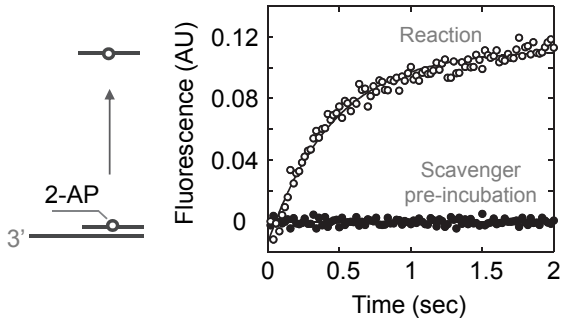

C

3' 25nt *	A^{max}	$K_{1/2}^{Ded1p}$(μM)	H	A^{max}	$K'_{1/2}^{ATP}$(mM)	H
10 bp	0.99 ± 0.07	0.57 ± 0.03	3.0 ± 0.4	0.91 ± 0.02	0.19 ± 0.01	1.2 ± 0.1
13 bp	0.61 ± 0.08	0.68 ± 0.05	4.2 ± 1.1	0.65 ± 0.08	0.62 ± 0.07	1.8 ± 0.3
16 bp	0.25 ± 0.03	0.69 ± 0.06	3.4 ± 0.7	0.41 ± 0.16	1.3 ± 0.5	1.9 ± 0.8
19 bp	0.04 ± 0.01	0.75 ± 0.12	3.1 ± 1.0	0.09 ± 0.05	3.4 ± 1.0	2.0 ± 1.0

D

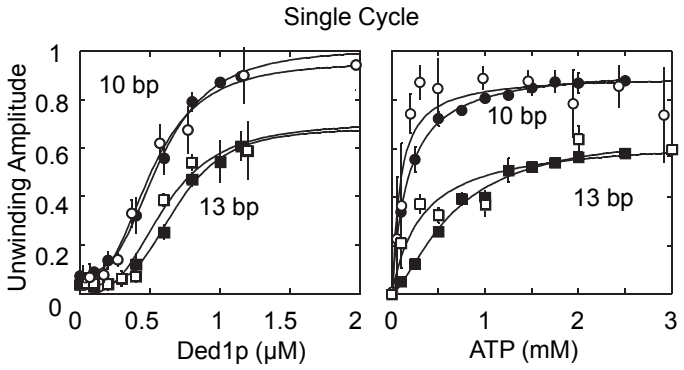

E

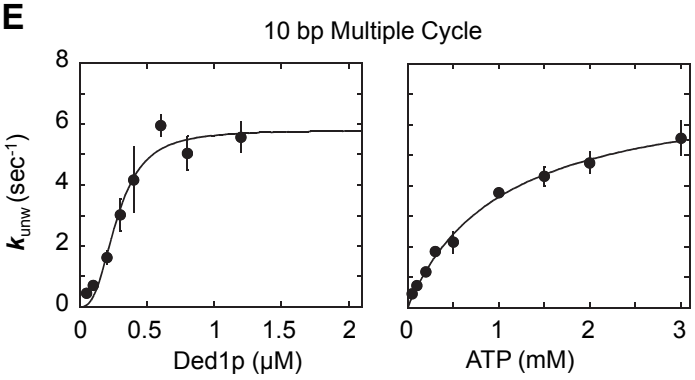

F

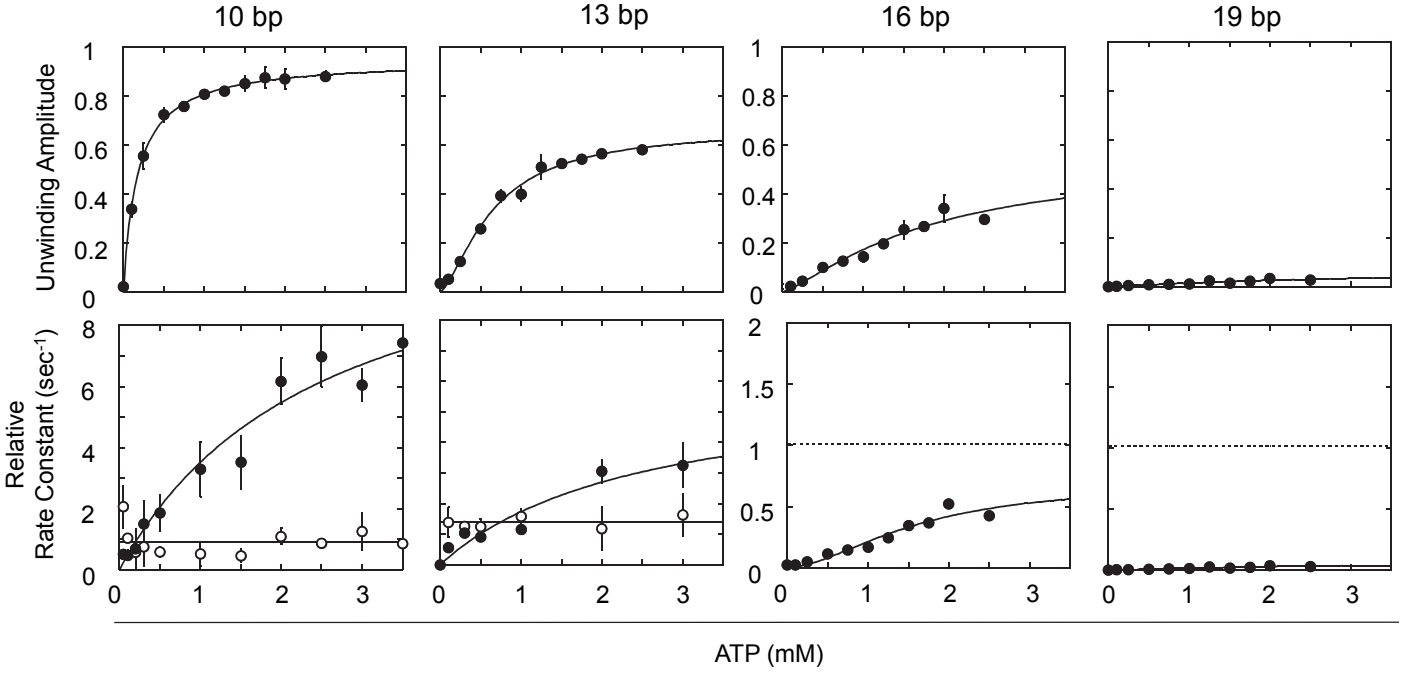

Supplementary Figure S5

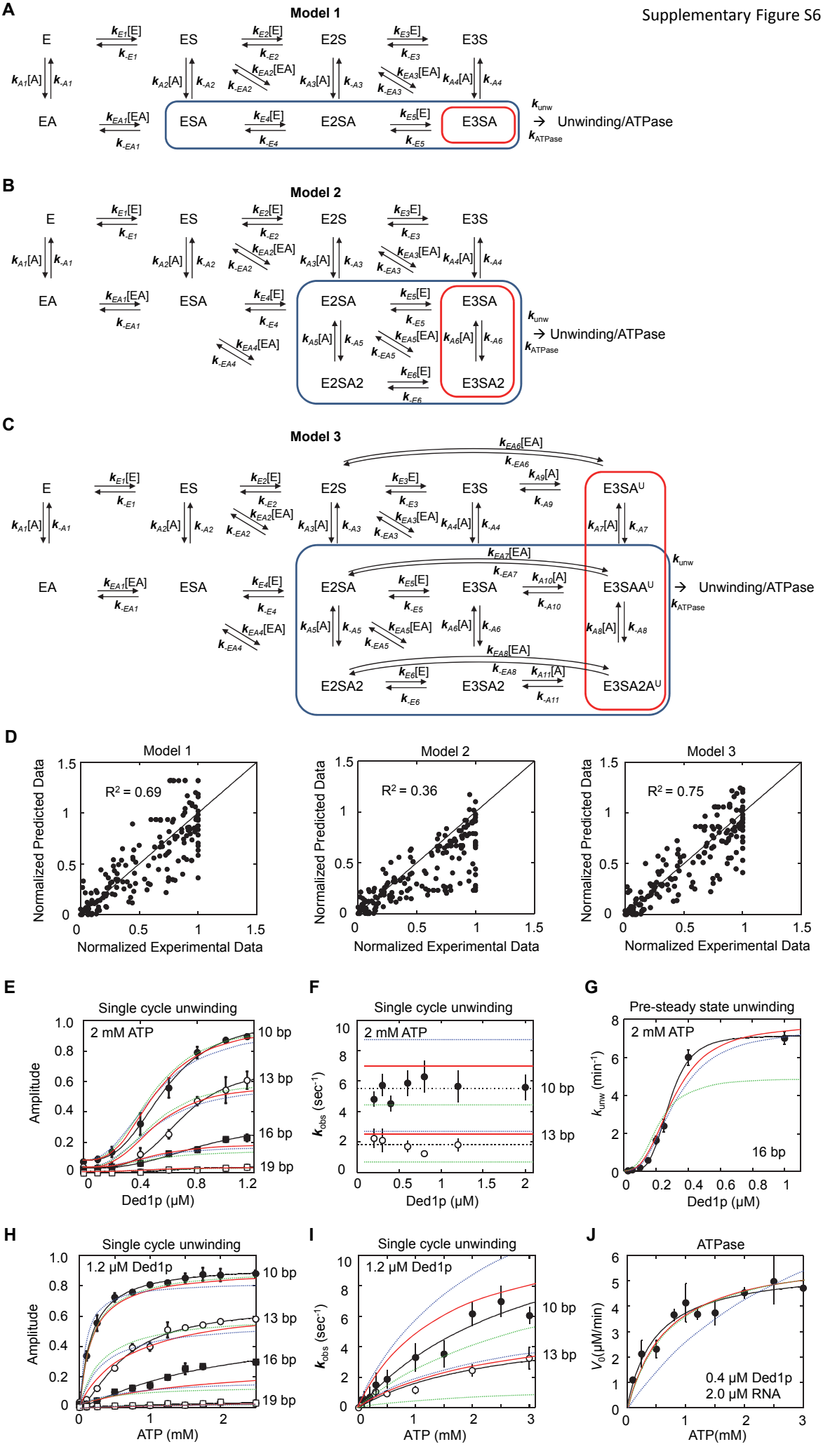
A
Model 1
E
ES
E2S
E3S
EA
ESA
E2SA
E3SA
Unwinding/ATPase
B
Model 2
E2SA2
E3SA2
C
Model 3
E3SA^U
E3SAA^U
E2SA2A^U
D
Model 1
Model 2
Model 3
R² = 0.69
R² = 0.36
R² = 0.75
Normalized Predicted Data
Normalized Experimental Data
E
Single cycle unwinding
2 mM ATP
Amplitude
Ded1p (μM)
10 bp
13 bp
16 bp
19 bp
F
Single cycle unwinding
2 mM ATP
k_obs (sec⁻¹)
G
Pre-steady state unwinding
2 mM ATP
k_unw (min⁻¹)
16 bp
H
Single cycle unwinding
1.2 μM Ded1p
ATP (mM)
I
Single cycle unwinding
1.2 μM Ded1p
J
ATPase
V0(μM/min)
0.4 μM Ded1p
2.0 μM RNA
ATP(mM)

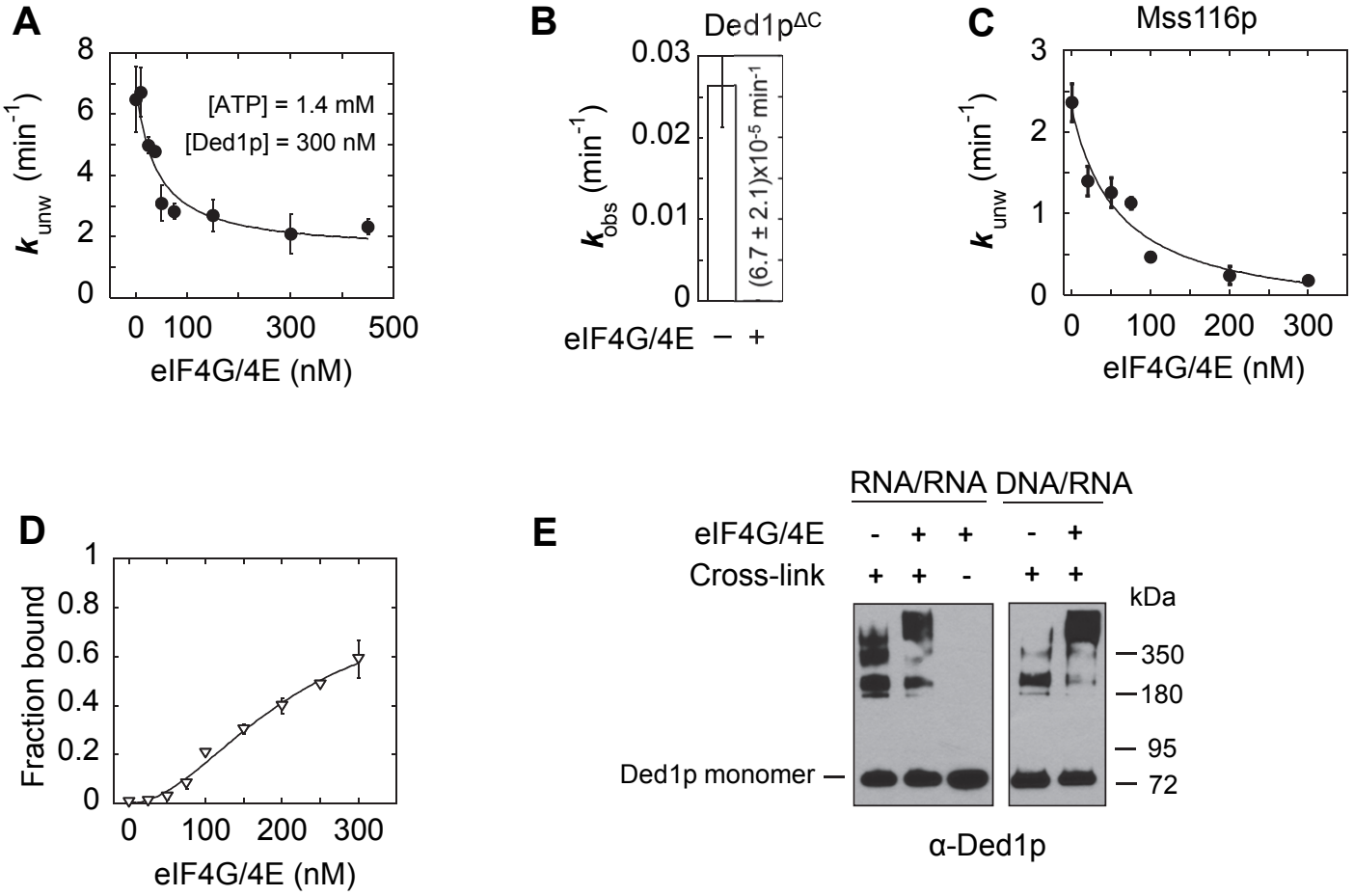

Supplementary Figure S7

Captions, Supplementary Figures

Figure S1 *(corresponds to Figure 1)*

Ded1p helicase domains and mutations used in this study. Helicase core: 93-535, N-terminus: 1-92, C-terminus:536-606. Characteristic helicase motifs are colored according to biochemical function: red, ATP binding and hydrolysis; blue, RNA binding; green, coordination between RNA and ATP binding sites (Putnam and Jankowsky, 2013a). The C-terminal deletion (Ded1p$^{\Delta C}$), the C-terminus (Ded1p-CT), and mutations in Ded1p^{DAAD} (E307A, motif II) and Ded1p^{R489A} (motif VI) are shown. The sequence logos show the sequence conservation in motifs II and VI among DEAD-box helicases (Putnam and Jankowsky, 2013a).

Figure S2 *(corresponds to Figure 2)*

(A) Representative EMSA for a steady state unwinding reaction with 100 nM Ded1p, 2 µM (0.5 nM ^{32}P-labeled) 10 bp duplex with a 25 nt single strand overhang, and 2 mM ATP/Mg^{2+}. The reaction included 10 µM single stranded top strand RNA to preclude re-annealing of the unwound duplex.

(B) Representative timecourse for the reaction shown in panel (A). The line indicates the best fit to a single exponential.

(C) Reaction scheme for control reactions examining the impact of single stranded top strand RNA on the pre-steady state observed unwinding rate constant.

(D) Impact of increasing concentrations of single stranded top strand RNA on the pre-steady state observed unwinding rate constant (k_{obs}). Reactions were performed as in panel (A), but without unlabeled duplex RNA. No significant inhibition of the reaction is observed up to 12 µM of the single stranded RNA.

(E) Impact of Ded1p concentration on turnover rate constant ($\boldsymbol{k}_{cat}$) of steady state unwinding reactions for a 10 bp duplex with 25 nt unpaired region 3' to duplex. Values are converted from the data shown in Figure 2A. The solid line marks a trend, the dashed line indicates the dependence of $\boldsymbol{k}_{cat}$ on the Ded1p concentration expected for a monomeric enzyme.

(F) Impact of Ded1p concentration on turnover rate constant ($\boldsymbol{k}_{cat}$) of steady state unwinding reactions for a 13 bp duplex with 25 nt unpaired region 3' to duplex. Values are converted from the data shown in Figure 2A. The solid line marks a trend, the dashed line indicates the dependence of $\boldsymbol{k}_{cat}$ on the Ded1p concentration expected for a monomeric enzyme.

(G) Hill coefficients for pre-steady state unwinding reactions for different RNA substrates (listed in Suppl. Materials). Data points are averages of multiple independent measurements. Error bars represent one standard deviation.

(H) Reaction scheme for measuring functional binding Ded1p of single stranded RNA and DNA through competition with duplex substrate.

(J) Functional binding of 41 nt single stranded RNA and DNA to Ded1p, measured as indicated in panel (H). Reactions were performed with 0.5 nM RNA (16 bp duplex with 25 nt 3' ssRNA), 0.3 µM Ded1p, 2 mM ATP/Mg^{2+}, indicated concentrations of 41 nt single stranded RNA (black circles) or DNA (open circles). Unwinding rate constants were fit to a competitive binding isotherm, according to $k_{obs} = k_{obs}^{max} \cdot [Ded1p]/(K_{1/2} \cdot (1+[RNA \text{ or } DNA]/K_I) + [Ded1p])^{-1}$ (k_{obs}: observed unwinding rate constant; $K_{1/2}$: apparent functional binding constant of Ded1p to the duplex substrate (Fig.2B); K_I : apparent functional binding constant for RNA (K_I = 0.113 ± 0.029 µM) or DNA (K_I = 0.154 ± 0.027 µM)). Data points are averages from multiple independent measurements (N ≥ 3). Error bars represent one standard deviation.

(K) Hill coefficients for ATPase reactions with different RNA substrates (listed in Suppl. Materials). Reactions were conducted and Hill coefficients calculated as described in Fig.2D. Data points are averages of multiple independent measurements (N ≥ 3). Error bars represent one standard deviation.

Figure S3 *(corresponds to Figure 3)*

(A) Lengthening of an unpaired RNA region enables more Ded1p protomers to bind. Representative non-denaturing PAGE of Ded1p-RNA complexes with increasing concentrations of ADPNP. Ded1p (0.8 µM) was incubated with 0.5 nM^{32}P-labeled RNA substrate (indicated on the left) and increasing concentrations of ADPNP-Mg^{2+} for 60 min.

(B) Representative sucrose gradient fractionation of RNA substrates shown in panel (A) alone (black circles) and with Ded1p and ADPNP (red circles). Binding reactions were performed as described in panel (A). Solid curves represent best fits to a sum of Gaussian distributions, green traces indicate individual Gaussian distributions. Dashed lines indicate peak fraction numbers of protein markers sedimented under identical conditions (ovalbumin, tetramers: aldolase, catalase).

(C) Additional controls for helicase reactions with clamped loading protomers, as performed in Figure 3C. *Lane 1*: Ded1p was incubated in the presence of 50 µM ADPNP/Mg^2 and 2 mM ATP/Mg^{2+}. Compared to Figure 4C, lane 6, no significant amount super-shifted complex was formed during the unwinding reaction, indicating that Ded1p binding to the RNA during the reaction is negligible. *Lane 2:* Reaction as described in lane 1 were terminated with SDS before loading, confirming that the RNA

species represent protein-free RNA. *Lane 3*: Reaction described in Figure 3C, lane 6, but terminated with SDS before loading, indicating that removal of protein returned unwound RNA.
(E) Representative non-denaturing PAGE for clamping of Ded1p$^{\Delta C}$ (1 μM) to an RNA substrate (0.5 nM) with increasing concentrations of ADPNP-Mg^{2+} for 60 min.

Figure S4 *(corresponds to Figure 4)*

(A) Scheme for measuring association and dissociation rate constants for the Ded1p-ATP-Mg^{2+}on RNA by smFRET.

(B) Apparent dissociation rate constants (k_{off}) for the Ded1p-ATP-Mg^{2+} complex, determined from dwell times before bound ($P^{0.3}$+$P^{0.5}$) to free ($P^{0.8}$) transitions (Ded1p = 1 μM). The line shows the best fit to a horizontal line (k_{off} = 3.22 ± 0.16 s^{-1}), indicating that the dissociation rate constant does not depend on the ATP concentration.

(C) Scaling of apparent association rate constants ($k_{on,obs}$) for the Ded1p-ATP-Mg^{2+} complex with the ATP concentration. Values for k_{obs} were determined from dwell times before free ($P^{0.8}$) to bound ($P^{0.3}$+$P^{0.5}$) transitions (Ded1p = 1 μM). The line shows the best fit to a line, corresponding to k_{on}= 2.48 ± 0.11$mM^{-1}s^{-1}$, the second order association rate constant for binding of ATP to the Ded1p-RNA complex.

(D) Ratio of population of molecules in the $P^{0.3}$ vs. the $P^{0.5}$ as a function of the Ded1p concentration. Values were calculated from smFRET histograms for Ded1p-ATP-Mg^{2+}at increasing concentrations of Ded1p (ATP = 1 mM). The line shows the best fit to a binding isotherme. At low concentrations of Ded1p the ratio of the $P^{0.3}$ to the $P^{0.5}$ state depends on the concentration of Ded1p, but no significant changes are seen above [Ded1p] = 0.5 μM.

(E) Apparent dissociation rate constants (k_{off}) for the Ded1p-ATP-Mg^{2+} complex, determined from dwell times before bound ($P^{0.3}$+$P^{0.5}$) to free ($P^{0.8}$) transitions (ATP = 1 mM). The line shows the best fit to a horizontal line (k_{off}= 3.30 ± 0.07 s^{-1}), indicating that the dissociation rate constant does not depend on the Ded1p concentration.
(F) At [Ded1p] = 1 μM, ATP binding is rate limiting. Scaling of apparent association rate constants (k_{obs}) for the Ded1p-ATP-Mg^{2+} complex with the Ded1p concentration. Values for k_{obs} were determined from dwell times before free ($P^{0.8}$) to bound ($P^{0.3}$+$P^{0.5}$) transitions (ATP = 1 mM). The line shows the best fit to a binding isotherme, indicating no significant contribution of the Ded1p concentration to the observed binding rate constant above a concentration of Ded1p > 0.8 μM.

(G) RNA-stimulated ATPase activity for Ded1p (0.4 μM) as a function of the RNA concentration (16 bp duplex with 3' 25 ntssRNA) at 2 mM ATP-Mg^{2+}. Initial ATPase rates (V_o) were calculated as described in Fig.2D. Data points are averages from multiple independent measurements (N ≥3). Error bars represent one standard deviation. Data were fit according to $V_o = V^{max} \cdot [RNA]/(K_{1/2}^{RNA}+[RNA])$. $K_{1/2}^{RNA}$ is the apparent functional binding constant for this RNA substrate. $K_{1/2}^{RNA} = 0.053 \pm 0.008$ μM, $V^{max} = 4.43 \pm 0.28$ $\mu M^{-1}min^{-1}$.
(H) RNA-stimulated ATPase activity for Ded1p (0.4 μM) as a function of the ATP concentration (RNA = 2 μM, 16 bp duplex with 3' 25 ntssRNA). Data were obtained as in panel G. Data points are averages from multiple independent measurements (N ≥3). Error bars represent one standard deviation. $K_{1/2}^{ATP} = 0.49 \pm 0.11$ mM, $V^{max} = 5.57 \pm 0.37$ $\mu M^{-1}min^{-1}$, $\boldsymbol{k}_{cat}^{ATP} = 0.23 \pm 0.02$ s^{-1}.
(I) Representative smFRET histogram for 1 μM $Ded1p^{R489A}$ and 2.0 mM ATP-Mg^{2+}. Curves represent best fits to a Gaussian distribution. Gray traces indicate individual Gaussian distributions, black curves show the sum of individual distributions.
(J) Representative smFRETtime tracef or 1 μM $Ded1p^{R489A}$ and 2.0 mM ATP-Mg^{2}. Free RNA and Ded1p bound states are assigned as in Fig.4.
(K) Association and dissociation rate constants and associated equilibrium constants for ATP-Mg^{2+} to the Ded1p-RNA complex. For calculation of the parameters see Suppl. Methods.
(L) Fraction of transitions from the $P^{0.3}$ to $P^{0.8}$smFRET state for wild type Ded1p with 0.75, 1, and 2 mMATP-Mg^{2+} and for $Ded1p^{R489A}$ with 2 mM ATP-Mg^{2+}. The total number of transitions for each condition was N > 15,000).

Figure S5 *(corresponds to Figure 5)*
(A) Schemes for the processes occuring during pre-incubation and during the reaction under single cycle conditions.
(B) Representative timecourse for an unwinding reaction of a 10 bp duplex substrate measured by stopped flow fluorescence (open circles). The control (closed circles) shows the timecourse when the RNA scavenger is added at the same time as the labeled substrate.

(C) Parameters obtained from the fit of the data in **Figure 5C** (left Table) and **Figure 5E** (right table) to the Hill equation.
(D) Comparison of reaction amplitudes under single cycle conditions obtained by EMSA (filled symbols) and by stopped flow fluorescence (open symbols) for 10 bp (circles) and the 13 bp (squares) duplex

substrates. Left plot: scaling of reaction amplitudes with the Ded1p concentration (ATP =2 mM). Right plot: scaling of reaction amplitudes with the ATP concentration (Ded1p = 1.2 μM). Data points are averages from multiple independent measurements (N ≥ 3). Error bars represent one standard deviation.

(E) Unwinding rate constants for the 10 bp duplex substrate under multiple cycle conditions (without RNA scavenger) measured by stopped flow fluorescence. Unwinding rate constants were determined as in **Figure 5B**. Left plot: scaling of unwinding rate constants with the Ded1p concentration (ATP = 2 mM). Right plot: scaling of unwinding rate constants with the ATP concentration (Ded1p = 1.2 μM). Data points are averages from multiple independent measurements (N ≥ 3). Error bars represent one standard deviation.

(F) The duplex length impacts the ATP dependence of reaction amplitudes under single cycle conditions because the unwinding rate constant scales with the ATP concentration, but not the dissociation constant of Ded1p from the RNA. Upper plots: ATP dependence of reaction amplitudes under single cycle conditions (**Figure 5E**) for each duplex length tested. Lower plots: ATP dependence of unwinding rate constants (k_{unw}^{obs}, filled circles) for each duplex tested. The open circles represent the dissociation rate constants (k_{off}^{Ded1P}) calculated from the independently measured unwinding amplitudes and unwinding rate constants for the 10 and 13 bp substrates (**Figure 5D,E**). Reaction amplitude, unwinding rate constants, and dissociation rate constant are linked according to: $k_{unw}^{obs} = k_{off}^{Ded1p}$(Amplitude/(1-Amplitude)). k_{off}^{Ded1p} does not scale significantly with the ATP concentration, andk_{off}^{Ded1p} is similar for both duplex length, indicating that it also does not scale significantly with the duplex length. Accordingly, for the plots of the 16 bp and the 19 bp duplex, the $k_{off}^{Ded1p} = 1.01 \pm 0.18\ s^{-1}$ (indicated by the dotted line) was used to calculate unwinding rate constants from the reaction amplitudes.

Figure S6 *(corresponds to Figure 6)*

(A - C) Kinetic schemes for RNA binding, unwinding and ATPase activities of Ded1p with one (panel A), two (panel B), or three (panel C) ATP binding events (E: Ded1p protomers, S: RNA substrate, A: ATP). ATP binding to the unwinding protomer of Ded1p is labeled as A^U.Association and dissociation rate constants are indicated for Ded1p without ATP ($\boldsymbol{k}_E$) or with ATP ($\boldsymbol{k}_{EA}$). A negative sign indicates the dissociation step. Binding of ATP is indicated by ($\boldsymbol{k}_A$). Numbers following each rate constant indicate the binding step. Complexes associated with unwinding activity are framed in red, complexes associated with ATPase activity in blue.

(D) Visualization of quality of fits for each kinetic model above. For fitting parameters and quality of fit tests see Suppl. Methods and **Tables 1-4**. To visualize the quality of fit for each model, normalized experimental rates for ATPase and rate constants for unwinding assays are plotted versus the predicted value for each model. Both, experimental and predicted values were normalized by setting the maximum experimental value in each dataset to 1. Black lines represent a linear fit with a slope of 1 and an intercept set at zero (R^2: correlation coefficient).

(E-J) Experimental data overlaid with data generated for each model (Model 1: dashed blue line, Model 2: dashed green line, Model 3: solid red line. Plots are as follows: (E) Single cycle unwinding amplitudes versus Ded1p, (F) Single cycle unwinding rate constants versus Ded1p, (G) Pre-steady state unwinding rate constants versus Ded1p for the 16 bp duplex (H) Single cycle unwinding amplitudes versus ATP, (I) Single cycle unwinding rate constants versus ATP , (J) RNA excess ATPase rates versus ATP.

While model 1 globally shows only a slightly decreased quality of fit, compared to model 3 (panel D), model 3 describes the strand separation rate constants measured under single cycle conditions (panel I) and ATPase data (panel J) significantly better than model 1.

Figure S7 *(corresponds to Figure 7)*

(A) Unwinding of the RNA substrate used in **Figure 7A** at a constant concentration of Ded1p (300 nM), 1.4 mM ATP and increasing concentrations of eIF4G/E, as indicated. Data points are averages from multiple independent measurements (N ≥ 3). Error bars indicate one standard deviation. The data show that leveling of the unwinding rate constants at increasing eIF4G/E is not restricted to low ATP concentrations.

(B) Effect of eIF4G/E (300 nM) on duplex unwinding by Ded1p$^{\Delta C}$ (300 nM). Unwinding rate constants were determined with the substrate used in panel (A) at 0.4 mM ATP. Addition of eIF4G/E decreases the unwinding rate constant by roughly three orders of magnitude, consistent with competition of eIF4G/E and Ded1p$^{\Delta C}$ for the RNA.

(C) Unwinding of the RNA substrate used in **Figure 7A** at a constant concentration of Mss116p (30 nM), 2 mM ATP and increasing concentrations of eIF4G/E, as indicated. Data points are averages from multiple independent measurements (N ≥ 3).Error bars represent one standard deviation. The data show that leveling of the unwinding rate constants at increasing eIF4G/E is not restricted to low ATP concentrations. Addition of increasing concentrations of eIF4G/E inhibits the unwinding by Mss116p virtually completely, thus indicating competition between eIF4G/E and Mss116p for the RNA.

(D) Equilibrium binding of eIF4G/E to the RNA (1 nM) used in panels (A-C). Reactions conditions were identical to those for unwinding. Data points are averages from multiple independent measurements (N ≥ 3). Error bars represent one standard deviation. The line represents a fit to the Hill equation ($K_{1/2}$ = 208 ± 54 nM, H = 1.9 ± 0.4). A Hill coefficient of H > 1 has also been observed for mammalian eIF4F binding to RNA (Kaye *et al*., 2009).

(E) Formaldehyde crosslinking of Ded1p (300 nM) and eIF4G (300 nM) with the RNA substrate (left panel) and the DNA-RNA chimeric substrate used in **Figure 7**. Proteins were visualized by western blot (α-Ded1p). Mobilities for the Ded1p monomer, oligomer and Ded1p-eIF4G complex are indicated.

SUPPLEMENTARY TABLES

Table S1 (*corresponds to Figure 6*)

	Model 1	Model 2	Model 3	Model 3 (No Cooperativity)
Relative Quality of Fit (Total)	1.69	1.66	1.00	1.64
Unwinding: Single Cycle	1.59	1.83	1.00	1.52
Unwinding: Pre-Steady State	1.00	1.88	1.08	1.22
ATPase	3.27	1.03	1.00	2.88

Chi-squared values obtained from global data simulations with Kintek Explorer for the entire model or individual data subsets, were normalized to the best fit in each data subset. A value of 1 indicates the best fit. Results for Model 3 without cooperativity between binding of first, second, third protomers of Ded1p are listed in the final column.

Table S2 (*corresponds to Figure 6*)

Model 1	Initial Parameters			Optimized Parameters		
REACTION STEP	k_{on} (μM^{-1} s^{-1})	k_{off} (s^{-1})	$K_{1/2}$ (μM)	k_{on}^{opt} (μM^{-1} s^{-1})	k_{off}^{opt} (s^{-1})	$K_{1/2}^{opt}$ (μM)
Ded1 Binding (-ATP)			$.54_{exp}$[a]			0.40 ± 0.04
E1 (k_{E1},k_{-E1})	6.1	3.3_{exp}[c]	.54	≤10*k_{off}	≥15	≥0.1
E2,4 (k_{E2},k_{-E2},k_{E4},k_{-E4})	6.1	3.3_{exp}[c]	.54	≤1.3*k_{off},≥0.01*k_{off}	≥15	≥0.8,≤100
E3,5 (k_{E3},k_{-E3},k_{E5},k_{-E5})	1.85	1_{exp}[d]	.54	≥6	0.57± 0.10	≤0.1
Ded1 Binding (+ATP)			0.32_{exp}[b]			0.045 ±.007
EA1 (k_{EA1},k_{-EA1})	10.3	3.3_{exp}[c]	.32	≥4*k_{off}	≥2.5	0.24 ± 0.04
EA2 (k_{EA2},k_{-EA2})	10.3	3.3_{exp}[c]	.32	≤40*k_{off},≥0.05*k_{off}	≥2.5	≥0.025,≤20
EA 3 (k_{EA3},k_{-EA3})	3.1	1_{exp}[d]	.32	≥0.7	≤0.69 ± 0.11	≤1
ATP Binding						
A1 (k_{A1},k_{-A1})	1	1590	1590_{exp}[e]	≥0.004	≥6	
A2-A4 (k_{A2-4},k_{-A2-4})	1	500	500_{exp}[g]	≥0.013	≥40	3300 ± 670
	k (s^{-1})	**H (experimental)**		**k (s^{-1})**	**H (predicted)**	
ATPase	$.23_{exp}$[c,f]	1.6_{exp}[b]		0.69 ± 11	1.66	
Unwinding						
10bp	14.8_{exp}[d]	3.0_{exp}[a,b,d]		20.1 ± 3.1	2.50	
13bp	2.8_{exp}[d]	4.2_{exp}[a]		3.5 ± 0.6	2.50	
16bp	$.85_{exp}$[d]	3.1_{exp}[a]		0.48 ± 0.1	2.50	
19bp	$.06_{exp}$[d]	3.1_{exp}[a]		0.08 ± 0.04	2.50	

Global data fit for model 1 (**Figure S6A**). Reaction steps correspond to those shown **Figure S6A.** Initial parameters estimated from experimental data are noted as "exp." Other initial parameters are extrapolated from experimental values. Parameters not allowed to float during simulations do not have optimized values listed. Optimized parameters are listed with the standard error from global fitting or as a limit (obtained using Kintek Fitspace). Parameters not allowed to float during simulations do not have optimized values listed. Initial estimates of rate and equilibrium constants were determined from experimental data as described in Supplementary Materials.

Letters following the values indicate the experimental source as follows:

a) Amplitudes from single cycle unwinding reactions (**Figure 5E,G**)

b) pre-steady state unwinding reaction (**Figure 2B**) and ATPase reactions with Ded1p excess (**Figure 2D**)

c) smFRET data (**Figures 4C**, **S6A**, **4A,B**)

d) single cycle unwinding rate constants (**Figures 5D**,**F**, **S5D**)

e) ATP equilbrium binding (Putnam and Jankowsky, 2013)

f) RNA excess ATPase assays (**Figure S4C,D**)

g) ATP affinity measured under pre-steady state unwinding (ref)

Supplementary Table 3 (*corresponds to Figure 6*)

Model 2	Initial Parameters			Optimized Parameters		
REACTION STEP	**k_{on} ($\mu M^{-1} s^{-1}$)**	**k_{off} (s^{-1})**	**$K_{1/2}$ (μM)**	**k_{on}^{opt} ($\mu M^{-1} s^{-1}$)**	**k_{off}^{opt} (s^{-1})**	**$K_{1/2}^{opt}$ (μM)**
Ded1 Binding (-ATP)			$.54_{exp}$ [a]			0.48 ± 0.03
E1 (k_{E1},k_{-E1})	6.1	3.3_{exp} [c]	.54	≤2*k_{off}	≥10	≥0.5
E2,4 ($k_{E2,4}$,$k_{-E2,4}$)	6.1	3.3_{exp} [c]	.54	≤5*k_{off},≥0.2*k_{off}	≥10	≥0.2,≤5
E3,5,6 ($k_{E3,5-6}$,$k_{-E3,5-6}$)	1.85	1_{exp} [d]	.54	≥4	0.36 ± 0.05	≤ 0.1
Ded1 Binding (+ATP)			0.32_{exp} [b]			0.06 ± 0.01
EA1 (k_{EA1},k_{-EA1})	10.3	3.3_{exp} [c]	.32	≥4*k_{off}	≥1.5	0.25 ± 0.03
EA2,3,4 (k_{E2-4},k_{-E2-4})	10.3	3.3_{exp} [c]	.32	≤250*k_{off},≥0.1*k_{off}	≥1.5	≥0.004,≤10
EA 5 (k_{E5},k_{-E5})	3.1	1_{exp} [d]	.32	≥4	≤ 0.39 ± 0.02	≤0.4
ATP Binding						
A1 (k_{A1},k_{-A1})	1	1590	1590_{exp} [e]	≥0.004	≥6	---
A2-A4 (k_{A2-4},k_{-A2-4})	$.00205_{exp}$ [c]	2.97_{exp} [c]	1440_{exp} [c]	---	---	---
A5,A6 (k_{A5-6},k_{-A5-6})	$.0059_{exp}$ [c]	15.5_{exp} [c]	2600_{exp} [c]	---	---	---
	k (s^{-1})	**H (experimental)**		**k (s^{-1})**	**H (predicted)**	
ATPase	$.23_{exp}$ [c,f]	1.6_{exp} [b]		0.39 ± 0.02	1.83	
Unwinding						
10bp	14.8_{exp} [d]	3.0_{exp} [a,b,d]		≥90	2.8	
13bp	2.8_{exp} [d]	4.2_{exp} [a]		2.2 ± 0.2	2.8	
16bp	$.85_{exp}$ [d]	3.1_{exp} [a]		0.17± 0.02	2.8	
19bp	$.06_{exp}$ [d]	3.1_{exp} [a]		0.04 ± 0.03	2.8	

Global data fit for model 2 (**Figure S6B**). Reaction steps correspond to those shown **Figure S6B.** For further explanation see legend of **Table S2**.

Supplementary Table 4 (*corresponds to Figure 6*)

Model 3	Initial Parameter			Optimized Parameter		
REACTION STEP	k_{on} ($\mu M^{-1} s^{-1}$)	k_{off} (s^{-1})	$K_{1/2}$ (μM)	k_{on}^{opt} ($\mu M^{-1} s^{-1}$)	k_{off}^{opt} (s^{-1})	$K_{1/2}^{opt}$ (μM)
Ded1 Binding (-ATP)			$.54_{exp}$ [a]			0.52 ±0.1
E1 ($\mathbf{k}_{E1}$,$\mathbf{k}_{-E1}$)	6.1	3.3_{exp} [c]	.54	≤0.1*$\mathbf{k}_{off}$	≥10	≥10
E2,4 ($\mathbf{k}_{E2,4}$,$\mathbf{k}_{-E2,4}$)	6.1	3.3_{exp} [c]	.54	≤7*$\mathbf{k}_{off}$,≥0.01*$\mathbf{k}_{off}$	≥10	≥0.15,≤100
E2,4,5 ($\mathbf{k}_{E2,4-5}$,$\mathbf{k}_{-E2,4-5}$)	1.85	1_{exp} [d]	.54	≥40	0.92 ±0.04	≤ 0.02
Ded1 Binding (+ATP)			0.32_{exp} [b]			0.45 ± 0.07
EA1 ($\mathbf{k}_{EA1}$,$\mathbf{k}_{-EA1}$)	10.3	3.3_{exp} [c]	.32	≥2.5*$\mathbf{k}_{off}$	≥10	0.38±0.06
EA2-5 ($\mathbf{k}_{EA2-5}$,$\mathbf{k}_{-EA2-5}$)	10.3	3.3_{exp} [c]	.32	≤5*$\mathbf{k}_{off}$,≥0.1*$\mathbf{k}_{off}$	≥10	≥0.2,≤10
EA 6-8 ($\mathbf{k}_{EA6-8}$,$\mathbf{k}_{-EA6-8}$)	3.1	1_{exp} [d]	.32	≥7	≤ 0.37 ±0.02	≤0.05
ATP Binding						
A1 ($\mathbf{k}_{A1}$,$\mathbf{k}_{-A1}$)	1	1590	1590_{exp} [e]	≥0.005	≥8	---
A2-A4,A7 ($\mathbf{k}_{A2-4,7}$,$\mathbf{k}_{-A2-4,7}$)	$.00205_{exp}$ [c]	2.97_{exp} [c]	1440_{exp} [c]	---	---	---
A5,A6,A8 ($\mathbf{k}_{A5-6,8}$,$\mathbf{k}_{-A5-6,8}$)	$.0059_{exp}$ [c]	15.5_{exp} [c]	2600_{exp} [c]	---	---	---
A9-11 ($\mathbf{k}_{A9-11}$,$\mathbf{k}_{-A9-11}$)	1	2500	$\geq 2500_{exp}$ [d]	≥0.014	≥40	3030±986
	k (s^{-1})	**H (experimental)**		**k (s^{-1})**	**H (predicted)**	
ATPase	$.23_{exp}$ [c,f]	1.6_{exp} [b]		0.37 ±0.02	1.75	
Unwinding						
10bp	14.8_{exp} [d]	3.0_{exp} [a,b,d]		15.6 ± 3.7	2.95	
13bp	2.8_{exp} [d]	4.2_{exp} [a]		2.95 ± 0.15	2.95	
16bp	$.85_{exp}$ [d]	3.1_{exp} [a]		0.47 ± 0.03	2.95	
19bp	$.06_{exp}$ [d]	3.1_{exp} [a]		0.07 ± 0.03	2.95	

Global data fit for model 3 (**Figure S6C**). Reaction steps correspond to those shown **Figure S6C.** For further explanation see legend of **Table S2**.

Supplementary Table 5 (*corresponds to Figure 7*)

eIF4G	Initial Parameter			Optimized Parameter		
REACTION STEP	k_{on} ($\mu M^{-1} s^{-1}$)	k_{off} (s^{-1})	$K_{1/2}$ (μM)	k_{on}^{opt} ($\mu M^{-1} s^{-1}$)	k_{off}^{opt} (s^{-1})	$K_{1/2}^{opt}$ (μM)
eIF4G + RNA	---	---	0.2_{exp} [h]	4.0 ± 1	9.5 ± 2	---
eIF4G-RNA + Ded1	---	---	$.3_{exp}$ [l]	≥65	≥10	0.15 ± 0.05
eIF4G + Ded1-RNA	---	---	0.02_{exp} [i]	≥300	≤0.15	≤0.0005
Unwinding	**k (s^{-1})**			**k (s^{-1})**		
13 bp, 5' - 25 nt	0.5_{exp} [i]			0.76 ± 0.01 [k] 0.17± 0.01 [l]		
With eIF4g	0.003_{exp} [l]			0.0029 ± 0.0011		

Global data fit for the Ded1p-eIF4G/E interaction **(Figure 7)**. Reaction steps correspond to those shown **Figure 7.** For further explanation see legend of **Table 2**.

Letters not explained in **Table 2** indicate:

h) eIF4G binding to RNA (**Figure S7D**)

i) Pre-steady unwinding reactions with Ded1p and eIF4G (**Figure 7A,B**)

k) Parameter given for ATP saturation.

l) Parameter for the ATP concentration used in the experiments (0.4 mM, **Figure 7**)

Supplementary Materials and Methods

OLIGONUCLEOTIDE SUBSTRATES

Radiolabeled and fluorescently labeled duplex substrates were purchased from Dharmacon (GE) and prepared as described (Yang & Jankowsky, 2005).

Duplexes with 25 nt 3' overhangs

Underlined regions correspond to the duplex region.
10bp duplex: 5'-AGC**A**CCGUAA-3' (radiolabeled top strand) and 3'-$(A_4C)_4$AAAAUUCGUGGCAUU-5'. Bold internal A was replaced with 2-AP for stopped flow fluorescence experiments.

13 bp duplex: 5'-AGC**A**CCGUAAAGA-3' (radiolabeled top strand) and 3'-('-$(A_4C)_4$AAAAUUCGUGGCAUUUCU-5'. Bold internal A was replaced with 2-AP for stopped flow fluorescence experiments.

16 bp duplex: 5'-AGCACCGUAAAGACGC-3' (radiolabeled strand) and 3'-$(A_4C)_4$AAAAUUCGUGGCAUUUCUGCG-5. These sequences are also used as the 16 and 41 nt single stranded sequences.

19 bp duplex: 5'-GCUGCGUCUUUACGGUGCU-3' (radiolabeled top strand) and 3'-($A_4C)_4$AAAAUCGACGCAGAAAUGCCACGA-5'.

Substrates with different length overhangs were generated by appending or deleting (A_4C) repeats. Blunt-end substrates did not contain any unpaired regions.

41 nt duplex with 24 nt overhang: 5'-UUAGUACGUCCCAGACAGCAUUGUACCCAGA GUCUGUACGG-3' and
3'-AACUACGACUACAGUAACUACGACAAUCAUGCAGGGUCUGUCGUAACAUGGG UCUCAGACAUGCC-5'.
These sequences are also used as 41 nt and 65 nt single stranded sequences.

36 nt blunt end duplex: 5'-AGCACCGUAAAGACGCAAUCAUGCAGGGUCUGUCAG-3' and 3'-UCGUGGCAUUUCUGCGUUAGUACGUCCCAGACAGUC-5.' These sequences are also used as 36 nt single stranded sequences.

Duplexes with 25 nt 5' overhangs

16 bp duplex: 3'-UCGUGGCAUUUCUGCG-5' (radiolabeled strand) and 5'-$(A_4C)_4$AAAAUAGCACCGUAAAGACGC-3'.

13 bp duplex: :3'-UCGUGGCAUUUCU-5' (radiolabeled strand) and 5'-$(A_4C)_4$AAAAUAGCACCGUAAAG-3'.

Single Stranded RNA

71 nt single stranded RNA: 5'-CCCAGACAGCAUUGUACCCAG AGUCUG UACGCGUCUUUACGGUGCUUA AAACAAAACAAAACAAAACAAAA-3'

73 nt Scavenger RNA: 5'-CCGUACAGGCUCUGGGUACAAUGCUUGUUUUUUUUCUGUCUGGGACGUA CUGCAUCAAUGACAUCAGCAUCAA-3'

25 nt single stranded RNA with hairpin: 5'-AGCAUUGUACCCAGAGUCUGUACGG-3' (hairpin duplex is underlined).

SmFRET substrates

Fluorescently labeled substrates were prepared as described (Yang et al., 2006, Liu et al., 2014). 3'-Cy3-AACUACGACUACAGUAACUACGACCGACGCAGAAAUGCCACGA-5' and 3'-Bio-UUUCGUGGCAUUUCUGCGUCG-Cy5-5'.

PROTEIN EXPRESSION AND PURIFICATION

Ded1p

Wild type Ded1p, Ded1p$^{\Delta C}$ (a.a. 1-535), Ded1p^{DAAD} (E307A), andDed1p^{R489A}were expressed and purified as described (Fairman et al., 2004; Yang and Jankowsky 2005), except that RNAses were added after cell lysis to remove contaminating bacterial RNA from the protein preparation, and that all protein storage buffers contained 50% glycerol. The C-terminus of Ded1p tagged with an N-terminal GST (GST-CT, a.a 536-604) was purified as described in Hilliker et al. (2011).

eIF4G/4E

Recombinant *S.cerevisae* eIF4G/4E complex was expressed and purified as described in Hilliker et al. (2011), except that the GST tag was removed with the Thrombin Cleavage Capture Kit (EMD Millipore). Homogeneity, concentration and stoichiometry of eIF4G to eIF4E were determined as described by Hilliker et al. (2011).

Equilibrium binding of eIF4G/4E to RNA

RNA binding was measured in a buffer containing 50 mM Tris–HCl (pH 8.0), 2.43 mM DTT, 0.01% (v/v) IGEPAL, 0.5 mM $MgCl_2$, 0.21 mM EDTA, 0.02% Triton-X100, 1 U/µl RNasin (Roche), 50 mM NaCl and 8% glycerol. Reactions were performed by incubating 0.2 µM eIF4G/4E, 1 nM radio-labeled 71 nt single-strand RNA, and 4 µM of the indicated unlabeled RNA or DNA as competitor for 10 minutes at 19 ^{o}C. Samples were applied to a native PAGE and binding was quantified as described (Kaye et al. 2009).

DATA ANALYSIS

Calculation of kinetic parameters from single molecule FRET measurements

Many observed smFRET transitions were close to the time resolution of the smFRET measurements (10 frames per second). To avoid bias in the data analysis due to undercounting short transition events, we combined dwell time analysis with steady state kinetics. This was possible because reactions were performed under steady state conditions. Observed FRET changes are shown in **Figure 4C**.The time-dependent changes of each state were described as follows:

$$\frac{d[\mathrm{P}^{0.8}]}{dt} = -(k_1 + k_{-3})[\mathrm{P}^{0.8}] + k_{-1}[\mathrm{P}^{0.5}] + k_3[\mathrm{P}^{0.5}] \qquad \text{Equation 1}$$

$$\frac{d[\mathrm{P}^{0.5}]}{dt} = k_1[\mathrm{P}^{0.8}] - (k_{-1} + k_2)[\mathrm{P}^{0.5}] + k_{-2}[\mathrm{P}^{0.3}] \qquad \text{Equation 2}$$

$$\frac{d[\mathrm{P}^{0.3}]}{dt} = k_2[\mathrm{P}^{0.5}] - (k_{-2} + k_3)[\mathrm{P}^{0.3}] + k_{-3}[\mathrm{P}^{0.8}] \qquad \text{Equation 3}$$

The steady state convention applied:

$$\frac{d[\mathrm{P}^{0.8}]}{dt} = 0 \qquad \text{Equation 4}$$

$$\frac{d[\mathrm{P}^{0.5}]}{dt} = 0 \qquad \text{Equation 5}$$

$$\frac{d[\mathrm{P}^{0.3}]}{dt} = 0 \qquad \text{Equation 6}$$

Finally, mass conservation was considered:

$$[\mathrm{P}^{0.8}] + [\mathrm{P}^{0.5}] + [\mathrm{P}^{0.3}] = [RNA]_0 \qquad \text{Equation 7}$$

From Eqs. 1-7, the expressions for the fraction of each FRET state as a function of the corresponding rate constants follow according to:

$$f_{0.8} = \frac{(k_3 + k_{-2})(k_{-1}k_{-2} + k_{-1}k_3 + k_3k_2)}{(k_3 + k_{-2} + k_2)(k_1k_{-2} + k_{-2}k_{-3} + k_3k_1) + (k_3 + k_{-3} + k_{-2})(k_{-1}k_{-2} + k_{-1}k_3 + k_3k_2)} \qquad \text{Equation 8}$$

$$f_{0.5} = \frac{(k_3 + k_{-2})(k_1k_{-2} + k_{-2}k_{-3} + k_3k_1)}{(k_3 + k_{-2} + k_2)(k_1k_{-2} + k_{-2}k_{-3} + k_3k_1) + (k_3 + k_{-3} + k_{-2})(k_{-1}k_{-2} + k_{-1}k_3 + k_3k_2)}$$

Equation 9

$$f_{0.3} = \frac{k_2(k_1k_{-2} + k_{-2}k_{-3} + k_3k_1) + k_{-3}(k_{-1}k_{-2} + k_{-1}k_3 + k_3k_2)}{(k_3 + k_{-2} + k_2)(k_1k_{-2} + k_{-2}k_{-3} + k_3k_1) + (k_3 + k_{-3} + k_{-2})(k_{-1}k_{-2} + k_{-1}k_3 + k_3k_2)}$$

Equation 10

The rate constants k_1, $k_2$and k_{-3}represent composite pseudo-first order association rate constants of binding of E-ATP to RNA. Values for each rate constant were determined by fitting the fraction of different FRET states as a function of ATP concentration using Eqs. 8-10.At the Ded1p concentrations used in the experiments, ATP binding was rate limiting (**Figure S4F**), and k_1, $k_2$and k_{-3} are linearly dependent on ATP concentration. Association rate constants were thus obtained according to:

$$k_1' = k_1[ATP] \quad \text{Equation 11}$$

$$k_2' = k_2[ATP] \quad \text{Equation 12}$$

$$k_{-3}' = k_{-3}[ATP] \quad \text{Equation 13}$$

The second order association rate constants given in **Figure 4C** are corrected for the Ded1p concentrations used in the experiments.

Rate constants for the Ded1p^{R489A} mutation were calculated by considering $P^{0.5}$ and $P^{0.3}$ FRET states as a single bound state (**Figure S4I-L**). The reaction scheme becomes:

$$P^{0.8}\ (\text{unbound}) \leftrightarrow (P^{0.5} + P^{0.3})\ (\text{bound}) \quad \text{Scheme 1}$$

Observed association rate constants ($k^{on,obs}$) obtained from the dwell time correspond to k_1+ k_{-3}, and dissociation rate constants (k_{off}) correspond to k_{-1}+ k_3.

Global Data Fitting and Kinetic Modeling

Kinetic simulation of unwinding and ATPase activities was performed using the KinTek Global Kinetic Explorer program (Johnson et al., 2009). The simplest model to explain the oligomerization of Ded1p required binding of 3 protomers of Ded1p (E) to RNA (S):

$$E + S \leftrightarrow ES + E \leftrightarrow E2S + E \leftrightarrow E3S \qquad \text{Scheme 2}$$

We considered several models for ATP utilization by the Ded1p trimer (**Figure S6A-C**).In model 1, a single ATP promotes unwinding and ATPase activity (**Figure S6A**), in model 2, two ATP promote unwinding and ATPase activities (**Figure S6B**), and in model 3, two protomers on the single stranded RNA bind and hydrolyze 2 ATP units, while a third unit of ATP binds to the unwinding protomer of Ded1p and promotes unwinding (**Figure 6C**). Only in model 3 ATPase and unwinding activities are separated between the loading and unwinding protomers.

Global fitting was performed on 16 data sets including multiple cycle unwinding (**Figure 2B**, **Figure S5D**), single cycle unwinding amplitudes and rates (**Figure 5B-E**, **Figure S5C,E**), and ATPase activity (**Figure 2D, Figure S4G,H**). Global fitting was conducted by alternating combinations of fixed and floated variables until the overall fit of the model did not improve further for multiple iterations. Initial parameters and the final calculated parameters of the respective models are listed in **Tables S2-4**.

The overall quality of fit was assessed through chi-squared values for the total model provided by the KinTek program. These chi-squared values were normalized to the best fit between the three models and for each data subset. These values are summarized in **Table S1**.

To visually assess the quality of fit for the different models, experimental data were plotted versus values predicted with the model (**Figure S6D**). In addition, we overlaid data calculated with the models with experimental data sets (**Figure S6E-J**).

Initial values of rate and equilibrium constants were determined from experimental data as described below and as given in **Tables S2-4**.

Determination of initial parameters for unwinding and ATPase rate reactions

ATPase turnover rate constants (k_{cat}) were determined from steady state ATPase assays (**Figure S4G,H**), by smFRET (**Figure 4**).

Unwinding rate constants were considered irreversible for all reactions. RNA strand annealing, where applicable, was eliminated in the initial determination of unwinding rate constants (Yang and Jankowsky, 2005). Unwinding rate constants for the 10 and 13 duplexes were determined under single cycle conditions (**Figures 5,S5**). Dissociation rate constants, k_{off}^{Eunw} (**Figures 5, S5F**) were calculated according to:

$$Amplitude^{obs} = \frac{k^{unw,obs}}{k^{unw,obs} + k_{off}{}^{Eunw}} \qquad \text{Equation 14}$$

ATP saturation could not be experimentally accomplished, but a minimum equilibrium dissociation constant of $K_{1/2}{}^{ATP} > 3$ mM was required for an adequate data fit. Using this limit, apparent maximum unwinding rate constants k'^{max} were determined according to:

$$k^{obs} = \frac{k^{max}[ATP]}{[ATP] + K_{1/2}{}^{ATP}} \qquad \text{Equation 15}$$

k^{obs} is the observed unwinding rate constant , k^{max} is the unwinding rate constant at ATP saturation, and $K_{1/2}{}^{ATP}$ is the ATP equilibrium dissociation constant.

It was not necessary to include unwinding by monomeric or dimeric Ded1p in final modeling. In fact, global fitting with rate constants of $k^{unw} > 0.005 s^{-1}$ for monomeric and dimeric Ded1p significantly decreased the quality of the fit and were thus not considered in the modeling.

Determination of initial parameters for ATP Binding

For model 1, ATP binding to the Ded1p-RNA complex was determined from previously published values for unwinding and ATPase assays (Putnam and Jankowsky, 2013a). For models 2 and 3, binding of ATP to the single stranded Ded1p protomers (A2-A8) were determined by the smFRET experiments (**Figure 4**). Association and dissociation rate constants for binding of the first ($k_{A2,3,4,7}$,$k_{\text{-}A2,3,4,7}$) and second ATP ($k_{A5,6,8}$, $k_{\text{-}A5,6,8}$) were set identical, regardless of the oligomeric state of Ded1p. During fitting, ATP binding rate constants determined by smFRET were fixed and not optimized. Binding equilibrium constants of ATP to the unwinding unit ($K_{1/2}^{A9\text{-}A11}$) were initially set at $K_{1/2}^{ATP}$= 3 mM, as noted above. Best fit results during global fitting were obtained with ATP association rate constants ($k_{A9\text{-}11}$) significantly greater than the unwinding rate constant for the 10 bp duplex.

Determination of initial parameters for RNA binding

Equilibrium dissociation constants were determined from unwinding assays for Ded1p to RNA without ATP ($K_{1/2}^{Ded1p}$ = 0.54 µM, **Figure 5C**) and with ATP ($K_{1/2}^{Ded1p\text{-}ATP}$ = 0.32 µM, **Figure 2B**). In the absence of cooperativity (model 3) $K_{1/2}^{Ded1p}$ =$K_{1/2}^{E1}$= $K_{1/2}^{E2}$= $K_{1/2}^{E3}$. Considering cooperativity (models 2,3), the overall dissociation constant obtained from the Hill Equation with H = 3 is equivalent to the cubic root of the product of the individual constants for each step (Scheme 2):

$$K_{1/2}{}^{Ded1p} = \sqrt[3]{(K_{1/2}{}^{E1} K_{1/2}{}^{E2} K_{1/2}{}^{E3})}$$

Equation 16

During global fitting, individual dissociation constants were not sufficiently constrained by the data. However, the overall dissociation constants with or without ATP ($K_{1/2}^{Ded1p}$) and limits for the individual steps were well constrained by the data. For this reason, only an overall dissociation constant for RNA binding to Ded1p with and without ATP is given in the final model (**Figure 6**). We note that cooperativity between the Ded1p protomers is required for a good overall fit of the data. For comparison, the overall quality of the fit without cooperativity are included in **Table S1**.

A composite dissociation rate constant ($\boldsymbol{k}_{off}^{Eunw}$**=** 1 s^{-1}) for the unwinding unit with and without ATP ($\boldsymbol{k}_{\text{-}EA6,7,8}$ $\boldsymbol{k}_{\text{-}E3,5,6}$) was determined from Eq. 14. Dissociation of Ded1p·ATP was measured by smFRET ($\boldsymbol{k}_{off}$≤

3.3 $s^{-1,}$ corresponds to $\boldsymbol{k}_{EA1,2,3,4}$, **Figure S4E**). This dissociation rate constant could represent dissociation of the Ded1p trimer, but not of the individual, loading protomers of Ded1p. Dissociation rate constants of the loading protomers without ATP were not directly accessible, and were initially set at $\boldsymbol{k}_{E1,2,4} = 3.3\ s^{-1}$. Association rate constants were not directly measured for Ded1, but limits could be reliably estimated, considering that ATP binding at 1 mM ATP is rate limiting at Ded1p concentrations of [Ded1p] ≥0.3 μM. Since Ded1p at 50 nM promotes association at roughly half of this rate constant, we estimated a bimolecular Ded1passociation rate constant of $\boldsymbol{k}^{\mathbf{on}} \approx 40\ \mu M^{-1}\ s^{-1}$.

Global fitting of the eIF4G/E-Ded1p interaction

The interaction of Ded1p and eIF4G/E was modeled by adding steps for eIF4G binding in the presence of RNA to model 3 (**Figure S7**). Global fitting was performed on 4 data sets (**Figure 7A,B**). Data were fit at a constant ATP concentration (0.4 mM), and binding of ATP to the Ded1p-eIF4G complex was not explicitly included. In the absence of eIF4G the unwinding rate constant for the 13 bp duplex with a 5' single stranded overhang was determined to be approximately 6 fold smaller then rate constants for the 13 bp duplex with a 3' single stranded overhang, consistent with the pre-steady state unwinding measurements under the conditions in **Figure 7E** ($\boldsymbol{k}^{unw,13\text{-}5'} = 0.8 \pm 0.1\ min^{-1}$, $\boldsymbol{k}^{unw,13\text{-}3'} = 4.7 \pm 1.4\ min^{-1}$). RNA unwinding in the presence of eIF4G ($\boldsymbol{k}^{unw,eIF4G}$) and equilibrium and rate constants for the binding of eIF4G were allowed to float. The results of the modeling are summarized in **Table S5**.

Supplementary References

Kaye, N.M., Emmett, K.J., Merrick, W.C., Jankowsky, E., (2009) Intrinsic RNA binding by the eukaryotic initiation factor 4F depends on a minimal RNA length but not on the m7G cap. J. Biol. Chem. 284, 17742 - 17750

Johnson, K. A., Simpson, Z. B., and Blom, T. (2009) Global Kinetic Explorer: A new computer program for dynamic simulation and fitting of kinetic data, Anal Biochem 387, 20-29.